Progress In Electromagnetics Research M, Vol. 63, 47–58, 2018

Analytical Solution of Metal Nanowires at Visible and Near-Infrared Wavelength

Zhong Wang, Xiaopan Cao, Aning Ma, Yuee Li, and Qingguo Zhou*

Abstract—Metal nanowires have drawn much attention due to the highly confined electromagnetic waves and relatively low propagation loss. With the increasing application potentials, we desire deeper insight into the mode behavior guided by metal nanowires for routing and controlling SPPs modes. Here, we apply the analytical solution for analyzing SPPs modes of metal nanowires. Single mode propagation condition and modes number are studied based on the analytical model. A universal formula of field diameters for all guided modes is presented, and mode field diameters are investigated. Finally, the intensity profiles of allowed guided modes are studied for specific dimensions.

1. INTRODUCTION

Surface plasmon polaritons (SPPs) confined by micro/nano-metallic configurations currently attract extensive interest. SPPs have been identified as promising building blocks for the next-generation integrated optical components [1], circuits [2] and membrane units [3, 4]. So far, many various types of practical SPPs waveguides have been proposed with the advance of micro-fabrication techniques, among which metallic nanowires are typical one-dimension waveguide structures with relatively low losses at visible and near-infrared spectral range. They show large application potentials in the plasmonic circuits, such as waveguides [5–7], resonators [8], nanoantennas [9, 10], optical routers [11, 12], logic gates [13] and THz photodetectors [14, 15].

The numerical method [5, 16] has been used for analyzing mode characteristics and designing metal nanowires. However, with the increasing application potentials of metal nanowires, we desire deeper insight into the mode behavior guided by metal nanowires for routing and controlling SPPs modes, and designing special optical circuits on sub-wavelength scale [17, 18]. The analytical method provides more information for understanding the mode cutoff characteristics, single-mode propagation and the number of modes etc by solving dispersion equations. To the best of our knowledge, the analytic method has not been used for studying SPPs modes supported by metal nanowires.

In this paper, an analytical model for SPPs modes supported by metal nanowire is studied. The dispersion relation for SPPs modes is obtained by solving the classical Helmholtz equations, and the eigen modes are classified by periodic azimuthal field distribution. To confirm the accuracy of our method, we calculate the effective indexes of TM modes and HE modes at 633 nm using our proposed analytical model and COMSOL Multiphysics. COMSOL Multiphysics is a popular numerical simulation tool for analyzing waveguides and gives precise results upon extremely fine mesh. For a specific waveguide structure, the fundamental mode changes over time according to a simple set of rules, and it is possible to anticipate future behavior of the field distribution. These simplifications of complex field distributions ease the signal processing requirements for the communication systems [19]. Therefore, waveguide structures for long-distance communication normally work on single-mode condition (all other modes are cutoff). Here, we analyze the cutoff radius a_c along with the relative permittivity

Received 14 September 2017, Accepted 10 November 2017, Scheduled 3 December 2017
* Corresponding author: Qingguo Zhou (zhouqg@lzu.edu.cn).
The authors are with the School of Information Science & Engineering, Lanzhou University, 222 Tianshui South Road, 730000, China.

of the cladding dielectric ε_{r2} for fundamental modes at several typical work wavelengths. The mode field diameter is also a vital parameter for designing the sub-wavelength plasmonic circuits. Based our analytical model, the mode field diameter of every SPPs mode can be calculated by solving an equation.

2. THEORETICAL MODEL OF METAL NANOWIRE

Metal nanowire could be regarded as an infinite long and straight metal nanowire with relative permittivity $\varepsilon_{r1} < 0$ embraced by rolling dielectric coaxial cylinders with relative permittivity $\varepsilon_{r2} > 0$, internal radius $R_{\text{core}} = a$ and external radius $R_{\text{cladding}} = \infty$. The theoretical model of the metal nanowire is illustrated in Fig. 1.

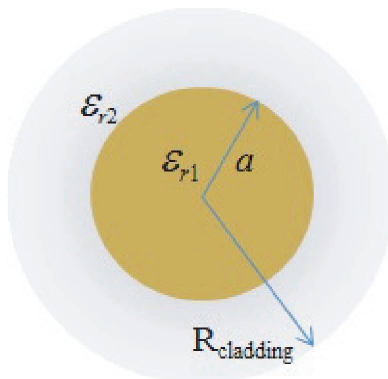

Figure 1. Theoretical model of the metal nanowire.

3. DISPERSION EQUATIONS OF METAL NANOWIRES

Considering optical modes propagating along z in SPPs waveguides, the longitudinal components in metal nanowires can be written in the forms

$$\begin{aligned} E_z &= E_z(x,y)e^{-j\beta z} \\ H_z &= H_z(x,y)e^{-j\beta z} \end{aligned} \tag{1}$$

Then, The longitudinal components in metal nanowires, E_{z1}, H_{z1} $(r < a)$ and E_{z2}, H_{z2} $(r > a)$ meet equations

$$\begin{aligned} \nabla_T^2 E_{z1} + \left(k_1^2 - \beta^2\right) E_{z1} = 0 \qquad (0 \le r \le a) \\ \nabla_T^2 H_{z1} + \left(k_1^2 - \beta^2\right) H_{z1} = 0 \qquad (0 \le r \le a) \end{aligned} \tag{2}$$

$$\begin{aligned} \nabla_T^2 E_{z2} + \left(k_2^2 - \beta^2\right) E_{z2} = 0 \qquad (r \ge a) \\ \nabla_T^2 H_{z2} + \left(k_2^2 - \beta^2\right) H_{z2} = 0 \qquad (r \ge a) \end{aligned} \tag{3}$$

where, $k_1 = k_0 n_1$, $k_2 = k_0 n_2$, $n_1 = \sqrt{\varepsilon_{r1}}$ and $n_2 = \sqrt{\varepsilon_{r2}}$ are refractive indexes of the metal core and the dielectric cladding respectively. In a cylindrical coordinate system, using method of variable separation and considering the natural cycle boundary conditions, Eqs. (2), (3) can be rewritten as

$$\begin{aligned} \frac{d^2 E_{z1}}{dr^2} + \frac{1}{r}\frac{dE_{z1}}{dr} + \left(n_1^2 k_0^2 - \beta^2 - \frac{m^2}{r^2}\right) E_{z1} = 0 \qquad (0 \le r \le a) \\ \frac{d^2 H_{z1}}{dr^2} + \frac{1}{r}\frac{dH_{z1}}{dr} + \left(n_1^2 k_0^2 - \beta^2 - \frac{m^2}{r^2}\right) H_{z1} = 0 \qquad (0 \le r \le a) \end{aligned} \tag{4}$$

$$\begin{aligned} \frac{d^2 E_{zd}}{dr^2} + \frac{1}{r}\frac{dE_{zd}}{dr} + \left(n_2^2 k_0^2 - \beta^2 - \frac{m^2}{r^2}\right) E_{z2} = 0 \qquad (r \ge a) \\ \frac{d^2 H_{z2}}{dr^2} + \frac{1}{r}\frac{dH_{z2}}{dr} + \left(n_2^2 k_0^2 - \beta^2 - \frac{m^2}{r^2}\right) H_{z2} = 0 \qquad (r \ge a) \end{aligned} \tag{5}$$

For SPPs modes supported by SPPs waveguides, $\frac{\beta}{k_0} > n_1^2, n_2^2$, and namely $k_0^2 n_1^2 - \beta^2 < 0, k_0^2 n_2^2 - \beta^2 < 0$. Define

$$\begin{aligned} U_1^2 &= a^2\left(\beta^2 - k_0^2 n_1^2\right) \\ U_2^2 &= a^2\left(\beta^2 - k_0^2 n_2^2\right) \\ V^2 &= U_1^2 - U_2^2 = a^2 k_0^2\left(n_2^2 - n_1^2\right) \end{aligned}$$

where $U_1^2 > 0$, $U_2^2 > 0$, then Eqs. (4), (5) are imaginary argument Bessel equations, and the solutions are (considering limitation of fields at $r = 0$ and $r \to \infty$ and $E_{z1} = E_{z2}|_{r=a}$, $H_{z1} = H_{z2}|_{r=a}$)

$$\begin{aligned} E_{z1} &= A' \frac{I_m\left(\frac{U_1}{a} r\right)}{I_m(U_1)} e^{jm\varphi} e^{-j\beta z} \\ H_{z1} &= B' \frac{I_m\left(\frac{U_1}{a} r\right)}{I_m(U_1)} e^{jm\varphi} e^{-j\beta z} \end{aligned} \tag{6}$$

$$\begin{aligned} E_{z2} &= A' \frac{K_m\left(\frac{U_2}{a} r\right)}{K_m(U_2)} e^{jm\varphi} e^{-j\beta z} \\ H_{z2} &= B' \frac{K_m\left(\frac{U_2}{a} r\right)}{K_m(U_2)} e^{jm\varphi} e^{-j\beta z} \end{aligned} \tag{7}$$

Using longitudinal field methods, other components in metal and dielectric can be derived from E_z and H_z

$$\left.\begin{aligned} E_{r1} &= e^{-j\beta z}\left[\frac{j\beta A' a}{U_1} \frac{I'_m\left(\frac{U_1}{a} r\right)}{I_m(U_1)} - \frac{\omega\mu_0 m B' a^2}{U_1^2 r} \frac{I_m\left(\frac{U_1}{a} r\right)}{I_m(U_1)}\right] e^{jm\varphi} \\ E_{\varphi 1} &= e^{-j\beta z}\left[-\frac{\beta A' m a^2}{U_1^2 r} \frac{I_m\left(\frac{U_1}{a} r\right)}{I_m(U_1)} - \frac{j\omega\mu_0 B' a}{U_1} \frac{I'_m\left(\frac{U_1}{a} r\right)}{I_m(U_1)}\right] e^{jm\varphi} \\ E_{r2} &= e^{-j\beta z}\left[\frac{j\beta A' a}{U_2} \frac{K'_m\left(\frac{U_2}{a} r\right)}{K_m(U_2)} - \frac{\omega\mu_0 m B' a^2}{U_2^2 r} \frac{K_m\left(\frac{U_2}{a} r\right)}{K_m(U_2)}\right] e^{jm\varphi} \\ E_{\varphi 2} &= e^{-j\beta z}\left[-\frac{\beta A' m a^2}{U_2^2 r} \frac{K_m\left(\frac{U_2}{a} r\right)}{K_m(U_2)} - \frac{j\omega\mu_0 B' a}{U_2} \frac{K'_m\left(\frac{U_2}{a} r\right)}{K_m(U_2)}\right] e^{jm\varphi} \end{aligned}\right\} \tag{8}$$

$$\left.\begin{aligned} H_{r1} &= e^{-j\beta z}\left[\frac{j\beta B' a}{U_1} \frac{I'_m\left(\frac{U_1}{a} r\right)}{I_m(U_1)} + \frac{\omega\varepsilon_0 n_1^2 m A' a^2}{U_1^2 r} \frac{I_m\left(\frac{U_1}{a} r\right)}{I_m(U_1)}\right] e^{jm\varphi} \\ H_{\varphi 1} &= e^{-j\beta z}\left[-\frac{\beta B' m a^2}{U_1^2 r} \frac{I_m\left(\frac{U_1}{a} r\right)}{I_m(U_1)} + \frac{j\omega\varepsilon_0 n_1^2 A' a}{U_1} \frac{I'_m\left(\frac{U_1}{a} r\right)}{I_m(U_1)}\right] e^{jm\varphi} \\ H_{r2} &= e^{-j\beta z}\left[\frac{j\beta B' a}{U_2} \frac{K'_m\left(\frac{U_2}{a} r\right)}{K_m(U_2)} + \frac{\omega\varepsilon_0 n_2^2 m A' a^2}{U_2^2 r} \frac{K_m\left(\frac{U_2}{a} r\right)}{K_m(U_2)}\right] e^{jm\varphi} \\ H_{\varphi 2} &= e^{-j\beta z}\left[-\frac{\beta m B' a^2}{U_2^2 r} \frac{K_m\left(\frac{U_2}{a} r\right)}{K_m(U_2)} + \frac{j\omega\varepsilon_0 n_2^2 A' a}{U_2} \frac{K'_m\left(\frac{U_2}{a} r\right)}{K_m(U_2)}\right] e^{jm\varphi} \end{aligned}\right\} \tag{9}$$

Using the boundary conditions $E_{\varphi 1} = E_{\varphi 2}$, $H_{\varphi 1} = H_{\varphi 2}$ at the interface $r = a$, the dispersion equations can be obtained

$$\left\{\begin{aligned} &\frac{\beta A' m a^2}{U_1^2 r} \frac{I_m\left(\frac{U_1}{a} r\right)}{I_m(U_1)} + \frac{j\omega\mu_0 B' a}{U_1} \frac{I'_m\left(\frac{U_1}{a} r\right)}{I_m(U_1)} = \frac{\beta A' m a^2}{U_2^2 r} \frac{K_m\left(\frac{U_2}{a} r\right)}{K_m(U_2)} + \frac{j\omega\mu_0 B' a}{U_2} \frac{K'_m\left(\frac{U_2}{a} r\right)}{K_m(U_2)}\Big|_{r=a} \\ &\frac{\beta B' m a^2}{U_1^2 r} \frac{I_m\left(\frac{U_1}{a} r\right)}{I_m(U_1)} - \frac{j\omega\varepsilon_0 n_1^2 A' a}{U_1} \frac{I'_m\left(\frac{U_1}{a} r\right)}{I_m(U_1)} = \frac{\beta m B' a^2}{U_2^2 r} \frac{K_m\left(\frac{U_2}{a} r\right)}{K_m(U_2)} - \frac{j\omega\varepsilon_0 n_2^2 A' a}{U_2} \frac{K'_m\left(\frac{U_2}{a} r\right)}{K_m(U_2)}\Big|_{r=a} \end{aligned}\right. \tag{10}$$

4. SPPS MODES DISCUSSION

When $m = 0$, Eq. (10) can be separated to two independent groups of equations. For TM modes, the dispersion equations are

$$\frac{n_1^2 I_0'(U_1)}{U_1 I_0(U_1)} = \frac{n_2^2 K_0'(U_2)}{U_2 K_0(U_2)}$$

With $I_0'(x) = I_1(x) K_0'(x) = -K_1(x)$, rewriting to

$$\frac{n_1^2 I_1(U_1)}{U_1 I_0(U_1)} + \frac{n_2^2 K_1(U_2)}{U_2 K_0(U_2)} = 0 \tag{11}$$

For TE modes, the dispersion equations

$$\frac{I_0'(U_1)}{U_1 I_0(U_1)} = \frac{K_0'(U_2)}{U_2 K_0(U_2)}$$

With $I_0'(x) = I_1(x) K_0'(x) = -K_1(x)$, rewriting to

$$\frac{I_1(U_1)}{U_1 I_0(U_1)} + \frac{K_1(U_2)}{U_2 K_0(U_2)} = 0 \tag{12}$$

Because $\frac{I_1(U_1)}{U_1 I_0(U_1)} > 0$, $\frac{K_1(U_2)}{U_2 K_0(U_2)} > 0$, solutions of Eq. (12) cannot exist. So TE modes do not exist in circular cross-section metal nanowires.

When $m \neq 0$, Eq. (10) can be rewritten as

$$\begin{aligned} \frac{\beta A' m}{U_1^2} + \frac{j\omega\mu_0 B'}{U_1} \frac{I_m'(U_1)}{I_m(U_1)} &= \frac{\beta A' m}{U_2^2} + \frac{j\omega\mu_0 B'}{U_2} \frac{K_m'(U_2)}{K_m(U_2)} \\ \frac{\beta B' m}{U_1^2} - \frac{j\omega\varepsilon_0 n_1^2 A'}{U_1} \frac{I_m'(U_1)}{I_m(U_1)} &= \frac{\beta m B'}{U_2^2} - \frac{j\omega\varepsilon_0 n_2^2 A'}{U_2} \frac{K_m'(U_2)}{K_m(U_2)} \end{aligned} \tag{13}$$

And then, the following dispersion equation can be obtained

$$(\beta m)^2 \left(\frac{1}{U_1^2} - \frac{1}{U_2^2}\right)^2 = -k_0^2 \left(\frac{n_1^2}{U_1} \frac{I_m'(U_1)}{I_m(U_1)} - \frac{n_2^2}{U_2} \frac{K_m'(U_2)}{K_m(U_2)}\right) \left(\frac{1}{U_2} \frac{K_m'(U_2)}{K_m(U_2)} - \frac{1}{U_1} \frac{I_m'(U_1)}{I_m(U_1)}\right) \tag{14}$$

Equation (14) can be rewritten to

$$(\beta m)^2 \left(\frac{1}{U_1^2} - \frac{1}{U_2^2}\right)^2 = -k_0^2 \left(n_1^2 \xi_m - n_2^2 \eta_m\right) \left(\eta_m - \xi_m\right) \tag{15}$$

where

$$\xi_m = \frac{1}{U_1} \frac{I_m'(U_1)}{I_m(U_1)}, \eta_m = \frac{1}{U_2} \frac{K_m'(U_2)}{K_m(U_2)} \tag{16}$$

Equation (16) takes the form

$$\eta_m = \frac{n_1^2 + n_2^2}{2n_2^2} \xi_m \pm \left[\left(\frac{n_1^2 - n_2^2}{2n_2^2}\right)^2 \xi_m^2 + m^2 \frac{n_{eff}^2}{n_2^2} \left(\frac{1}{U_1^2} - \frac{1}{U_2^2}\right)^2\right]^{\frac{1}{2}} \tag{17}$$

where, $n_{eff} = \beta / k_0$ is the effective index. The positive sign yields EH modes and the minus sign corresponds to HE modes. And because

$$\xi_m = \frac{1}{U_1} \frac{I_m'(U_1)}{I_m(U_1)} = \frac{1}{U_1} \frac{\frac{m}{U_1} I_m(U_1) + I_{m+1}(U_1)}{I_m(U_1)} > 0$$

$$\eta_m = \frac{1}{U_2} \frac{K_m'(U_2)}{K_m(U_2)} = \frac{1}{U_2} \frac{-\frac{m}{U_2} K_m(U_2) - K_{m-1}(U_2)}{K_m(U_2)} < 0$$

$$\left[\left(\frac{n_1^2 - n_2^2}{2n_2^2}\right)^2 \xi_m^2 + m^2 \frac{n_{eff}^2}{n_2^2} \left(\frac{1}{U_1^2} - \frac{1}{U_2^2}\right)^2\right]^{\frac{1}{2}} > \left|\frac{n_1^2 + n_2^2}{2n_2^2} \xi_m\right|$$

Only minus sign yields a solution in Eq. (17). Then only HE modes are guided in metal nanowires. The dispersion equation of HE modes is

$$\eta_m = \frac{n_1^2+n_2^2}{2n_2^2}\xi_m - \left[\left(\frac{n_1^2-n_2^2}{2n_2^2}\right)^2 \xi_m^2 + m^2\frac{n_{eff}^2}{n_2^2}\left(\frac{1}{U_1^2}-\frac{1}{U_2^2}\right)^2\right]^{\frac{1}{2}} \tag{18}$$

An equivalent form of Eq. (18) is

$$\xi_m = \frac{n_1^2+n_2^2}{2n_1^2}\eta_m + \left[\left(\frac{n_1^2-n_2^2}{2n_1^2}\right)^2 \eta_m^2 + m^2\frac{n_{eff}^2}{n_1^2}\left(\frac{1}{U_1^2}-\frac{1}{U_2^2}\right)^2\right]^{\frac{1}{2}} \tag{19}$$

Using Eq. (16) and $U_1 = \sqrt{a^2k_0^2(n_{eff}^2 - n_1^2)}$, $U_2 = \sqrt{a^2k_0^2(n_{eff}^2 - n_2^2)}$ the solutions n_{eff} of Eq. (19) can be obtained, and then the characteristics of HE modes can be analyzed. All modes supported by metal nanowires can be discussed including single-mode propagation condition and the number of guided modes by metal nanowires by solving Eq. (11) and Eq. (19). We calculate the effective indexes using two methods including our analytical model and COMSOL Multiphysics (in bracket). The results are listed in Table 1. The relative permittivity of the dielectric material is $\varepsilon_{r2} = 1.45^2$ (SiO_2), and the permittivity of noble metal is using the measured value in [20]. The results indicate that our analytical method is correct, and further work based on our equations is treasured. TM, as the fundamental mode, is the only TM mode supported by the metal nanowire and always exists. However, all HE_m modes have cutoff conditions. When the radius a of the core is larger than 100 nm, our results are slightly different from COMSOL simulation data. It is because the radius of the cladding $R_{\text{cladding}} = 3\,\mu\text{m}$ is used for COMSOL simulation, while our analytical model uses $R_{\text{cladding}} = \infty$.

5. SINGLE MODE PROPAGATION

5.1. The Cutoff Radius

Now we consider the cutoff characteristics of SPPs modes supported by metal nanowires. The permittivity of metal changes with the working wavelength, so it is infeasible to discuss the cutoff frequency f or the cutoff wavelength λ. Here, we propose the cutoff radius a_c for metal nanowires, and the corresponding mode cuts off at the fixed work wavelength while the core radius meets the condition $a < a_c$. Therefore, the number of modes guided by nanowires can be tuned by adjusting the core radius of nanowires. Firstly, we deduce the dispersion equation under the cutoff condition.

When TM modes are cut off, $U_2 \to 0$, $U_1 \to V{=}V_c$, then

$$K_1(U_2) \sim \frac{1}{U_2}$$

$$K_0(U_2) \sim -\ln\left(\frac{U_2}{2}\right)$$

Rewriting Eq. (11) to

$$\frac{n_1^2 I_1(V_c)}{n_2^2 I_0(V_c)} = \frac{V_c}{\lim_{U_2\to 0} U_2^2 \ln(U_2/2)} \tag{20}$$

Because $\lim_{U_2\to 0} U_2^2 \ln(U_2/2) = 0$, Eq. (11) has no solution. It means that the TM mode (as the fundamental mode) always exists, but the effective index $n_{eff} = \beta/k_0$ becomes very large when the radius of nanowire $a \to 0$ (as shown in Table 1).

When HE modes are cut off, $n_{eff} = \beta/k_0 \to n_2$, $U_2 \to 0$ and $U_1 \to V$, then the modified Bessel functions have the following approximations

$$K_m(U_2) \sim \frac{(m-1)!}{2}\left(\frac{U_2}{2}\right)^{-m}$$

$$K_m'(U_2) = \frac{m}{U_2}K_m(U_2) - K_{m+1}(U_2) \sim -\frac{m!}{4}\left(\frac{U_2}{2}\right)^{-m-1}$$

Then, $\xi_m \sim \frac{1}{V_c}\frac{I'_m(V_c)}{I_m(V_c)}$, $\eta_m = \frac{1}{U_2}\frac{K'_m(U_2)}{K_m(U_2)} \sim -\frac{m}{U_2^2}$ and the dispersion equation under the cutoff condition is obtained

$$\left(\frac{n_1^2+n_2^2}{2n_2^2}\frac{1}{V_c}\frac{I'_m(V_c)U_2^2}{I_m(V_c)}+m\right)^2 = U_2^4\left(\frac{n_1^2-n_2^2}{2n_2^2}\right)^2\left[\frac{1}{V_c}\frac{I'_m(V_c)}{I_m(V_c)}\right]^2 + m^2\left(\frac{U_2^2}{U_1^2}-1\right)^2 \tag{21}$$

Solve Eq. (21) when the waveguide material parameters n_1, n_2 are specified, the cutoff frequency V_c of all HE modes can be acquired, and the single-mode propagation condition can be discussed. If the work wavelength λ is given, the cutoff radius can be calculated by using $a_c = \frac{\lambda_0 V_c}{2\pi\sqrt{(n_2^2-n_1^2)}}$. The metal nanowire works in the single-mode propagation condition when the core radius meets the requirement ($a < a_c$) (only TM_0 mode is guided in SPPs waveguide, and all HE modes are cut off).

Table 1. The effective index of TM and HE_m ($m = 1, 2, 3, 4, 5$) modes at $\lambda = 633$ nm ($\varepsilon_{r1} = -16.22 + i0.52$, Ag, $\varepsilon_{r2} = 1.45^2$).

a	TM	HE_1	HE_2	HE_3	HE_4	Number of Modes
20 nm	2.9680 (2.9680)	Cutoff	Cutoff	Cutoff	Cutoff	1
30 nm	2.3451 (2.3451)	Cutoff	Cutoff	Cutoff	Cutoff	1
40 nm	2.0816 (2.0816)	1.4560 (1.4560)	Cutoff	Cutoff	Cutoff	2
50 nm	1.9456 (1.9456)	1.4734 (1.4734)	Cutoff	Cutoff	Cutoff	2
60 nm	1.8655 (1.8655)	1.4969 (1.4969)	Cutoff	Cutoff	Cutoff	2
70 nm	1.8136 (1.8136)	1.5193 (1.5193)	Cutoff	Cutoff	Cutoff	2
80 nm	1.7775 (1.7775)	1.5376 (1.5376)	Cutoff	Cutoff	Cutoff	2
90 nm	1.7508 (1.7508)	1.5517 (1.5517)	Cutoff	Cutoff	Cutoff	2
100 nm	1.7303 (1.7303)	1.5623 (1.5623)	Cutoff	Cutoff	Cutoff	2
200 nm	1.6437 (1.6438)	1.5912 (1.5913)	1.4544 (1.4544)	Cutoff	Cutoff	3
300 nm	1.6154 (1.6159)	1.5895 (1.5900)	1.5130 (1.5135)	Cutoff	Cutoff	3
400 nm	1.6010 (1.6024)	1.5855 (1.5869)	1.5389 (1.5403)	1.4633 (1.4644)	Cutoff	4
500 nm	1.5922 (1.5949)	1.5818 (1.5848)	1.5505 (1.5535)	1.4984 (1.5013)	Cutoff	4
600 nm	1.5862 (1.5911)	1.5788 (1.5839)	1.5564 (1.5615)	1.5188 (1.5239)	1.4663 (1.4711)	5
700 nm	1.5819 (1.5895)	1.5763 (1.5843)	1.5594 (1.5675)	1.5311 (1.5392)	1.4913 (1.4993)	5

Table 2. The cutoff radius a_c of metal nanowires for five work wavelengths.

$\lambda(\varepsilon_r)$	Cutoff radius a_c (μm)			
	MgF_2 $\varepsilon_{r2} = 1.3767^2$	SiQ_2 $\varepsilon_{r2} = 1.45^2$	ITO $\varepsilon_{r2} = 1.842^2$	TiQ_2 $\varepsilon_{r2} = 2.7^2$
633 nm ($-16.22 + i0.52$, Ag)	50	38	24	12
785 nm ($-22.81 + i1.22$, Ag)	56	54	39	18
1064 nm ($-48.34 + i3.76$, Au)	122	99	77	46
1550 nm ($-132 + i12.65$, Au)	394	235	178	65
2000 nm ($-201.98 + i28.61$, Au)	510	348	220	92

Table 2 gives the calculated cutoff radius a_c at five typical work wavelengths $\lambda = 633$ nm, 785 nm, 1064 nm, 1550 nm and 2000 nm. Experimental values of the relative permittivity of Ag and Au [20] are used for our analysis, and four different substrates including MgF_2, SiQ_2, ITO and TiQ_2 are considered [5]. Fig. 2 gives curves of the cutoff radius along with the relative permittivity of the cladding dielectric. The metal nanowires with smaller radius are needed for single-mode propagation when the work wavelength decreases or the relative permittivity of the dielectric increases. When the work wavelength is fixed, the single-mode condition can be achieved by balancing the radius a and the cladding permittivity ε_{r2} of metal nanowires.

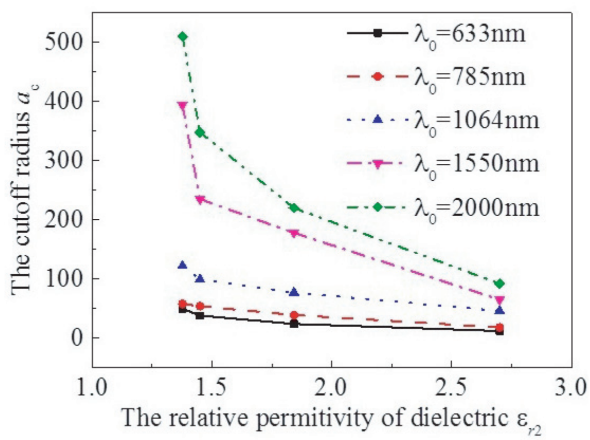

Figure 2. The cutoff radius along with the relative permittivity of the cladding dielectric.

The effective indexes for all SPPs modes guided by metal nanowires at $\lambda = 785$ nm, 1064 nm, 1550 nm and 2000 nm are shown in Tables 3, 4, 5, 6 using our analytical model. Fewer SPPs modes are supported by metal nanowires with smaller core radius at the fixed work wavelength. Fewer SPPs modes are guided by metal nanowires with fixed core radius at longer wavelength λ_0.

5.2. Modes Field Diameters

The mode field diameter is defined as D, when $r = D/2$, $E_{z2}|_{r=D/2} = \frac{1}{e}E_{z2\max}$. As a vital parameter of SPPs waveguides, the mode field diameter is the minimum spacing between neighboring nanowires for integrated optical circuits. The crosstalk of them cannot be neglected when the distance is smaller than D.

Considering Eq. (7), we have

$$\frac{K_m\left(D/2\sqrt{\beta^2 - k_0^2 n_2^2}\right)}{K_m\left(a\sqrt{\beta^2 - k_0^2 n_2^2}\right)} = \frac{1}{e} \tag{22}$$

Table 3. The effective index of TM and HE_m $(m = 1, 2, 3, 4)$ modes at $\lambda = 785\,\mathrm{nm}$ ($\varepsilon_{r1} = -22.81+i1.22$, Ag, $\varepsilon_{r2} = 1.45^2$).

a	20 nm	30 nm	40 nm	50 nm	60 nm	70 nm	80 nm	90 nm
TM	2.8742	2.2744	2.0213	1.891	1.8147	1.7653	1.7311	1.706
HE_1	Cutoff	Cutoff	Cutoff	Cutoff	1.4584	1.4676	1.4782	1.4885
HE_2	Cutoff	Cutoff	Cutoff	Cutoff	Cutoff	Cutoff	Cutoff	Cutoff
HE_3	Cutoff	Cutoff	Cutoff	Cutoff	Cutoff	Cutoff	Cutoff	Cutoff
Number of Modes	1	1	1	1	2	2	2	2
a	100 nm	200 nm	300 nm	400 nm	500 nm	600 nm	700 nm	
TM	1.6868	1.6062	1.58	1.5665	1.5583	1.5527	1.548	
HE_1	1.4978	1.5389	1.5452	1.5451	1.5437	1.5421	1.5405	
HE_2	Cutoff	Cutoff	1.4545	1.4834	1.5007	1.5106	1.5165	
HE_3	Cutoff	Cutoff	Cutoff	Cutoff	1.4523	1.4598	1.4768	
Number of Modes	2	2	3	3	4	4	4	

Table 4. The effective index of TM and HE_m $(m = 1, 2, 3, 4)$ modes at $\lambda = 1064\,\mathrm{nm}$ ($\varepsilon_{r1} = -48.34 + i3.76$, Au, $\varepsilon_{r2} = 1.45^2$).

a	20 nm	30 nm	40 nm	50 nm	60 nm	70 nm	80 nm	90 nm
TM	2.4765	2.0293	1.8457	1.7525	1.6981	1.663	1.6386	1.6205
HE_1	Cutoff	Cutoff	Cutoff	Cutoff	Cutoff	Cutoff	Cutoff	Cutoff
HE_2	Cutoff	Cutoff	Cutoff	Cutoff	Cutoff	Cutoff	Cutoff	Cutoff
Number of Modes	1	1	1	1	1	1	1	1
a	100 nm	200 nm	300 nm	400 nm	500 nm	600 nm	700 nm	
TM	1.6066	1.5477	1.5281	1.518	1.5117	1.5074	1.5043	
HE_1	1.4531	1.4731	1.4844	1.4892	1.4912	1.4921	1.4923	
HE_2	Cutoff	Cutoff	Cutoff	Cutoff	Cutoff	1.4524	1.4593	
Number of Modes	2	2	2	2	2	3	3	

Table 5. The effective index of TM and HE_m $(m = 1, 2)$ modes at $\lambda = 1550\,\mathrm{nm}$ ($\varepsilon_{r1} = -132 + i12.65$, Au, $\varepsilon_{r2} = 1.45^2$).

a	20 nm	30 nm	40 nm	50 nm	60 nm	70 nm	80 nm	90 nm
TM	2.1177	1.8199	1.7015	1.6421	1.6074	1.5847	1.5688	1.5569
HE_1	Cutoff	Cutoff	Cutoff	Cutoff	Cutoff	Cutoff	Cutoff	Cutoff
Number of Modes	1	1	1	1	1	1	1	1
a	100 nm	200 nm	300 nm	400 nm	500 nm	600 nm	700 nm	
TM	1.5477	1.5078	1.4943	1.4873	1.4829	1.4799	1.4777	
HE_1	Cutoff	Cutoff	1.4532	1.4563	1.4588	1.4606	1.4619	
Number of Modes	1	1	1	2	2	2	2	

By solving Eq. (22), mode field diameters of all SPPs modes can be calculated when the structure and materials parameters a, n_1, n_2 are given. $\vec{E}$ mode patterns for all supported modes by metal nanowires are presented in Fig. 3 ($\varepsilon_{r2} = 1.45^2$, $a = 30\,\mathrm{nm}$), Fig. 4 ($\varepsilon_{r2} = 1.45^2$, $a = 100\,\mathrm{nm}$), Fig. 5 ($\varepsilon_{r2} = 1.45^2$, $a = 300\,\mathrm{nm}$), and Fig. 6 ($\varepsilon_{r2} = 1.45^2$, $a = 700\,\mathrm{nm}$). Curves of mode field diameters with the work wavelengths are embedded. At the same time, various cladding dielectric including MgF_2, SiQ_2, ITO and TiQ_2 are considered.

Table 6. The effective index of TM and HE_m ($m = 1, 2$) modes at $\lambda = 2000$ nm ($\varepsilon_{r1} = -201.98 + i28.61$, Au, $\varepsilon_{r2} = 1.45^2$).

a	20 nm	30 nm	40 nm	50 nm	60 nm	70 nm	80 nm	90 nm
TM	2.1009	1.8063	1.6895	1.631	1.597	1.5749	1.5595	1.548
HE_1	Cutoff	Cutoff	Cutoff	Cutoff	Cutoff	Cutoff	Cutoff	Cutoff
Number of Modes	1	1	1	1	1	1	1	1
a	100 nm	200 nm	300 nm	400 nm	500 nm	600 nm	700 nm	
TM	1.5392	1.5011	1.4884	1.4818	1.4777	1.4749	1.4728	
HE_1	Cutoff	Cutoff	Cutoff	Cutoff	Cutoff	Cutoff	1.4518	
Number of Modes	1	1	1	1	1	1	2	

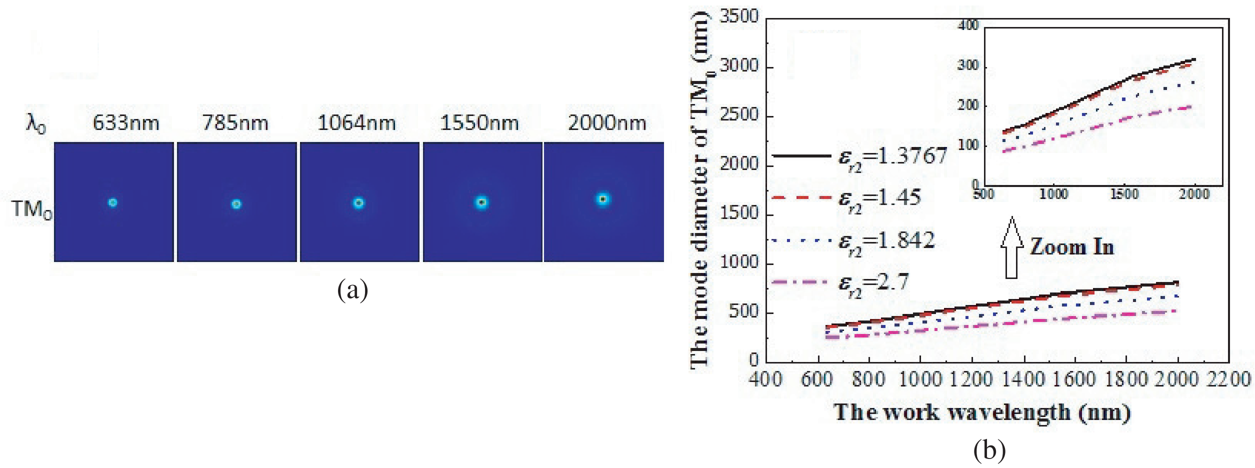

Figure 3. (a) $|E|$ mode patterns for all supported modes by metal nanowires with $a = 30$ nm and $\varepsilon_{r2} = 1.45^2$; (b) Curves of mode field diameters with the work wavelengths and permittivity of cladding dielectric.

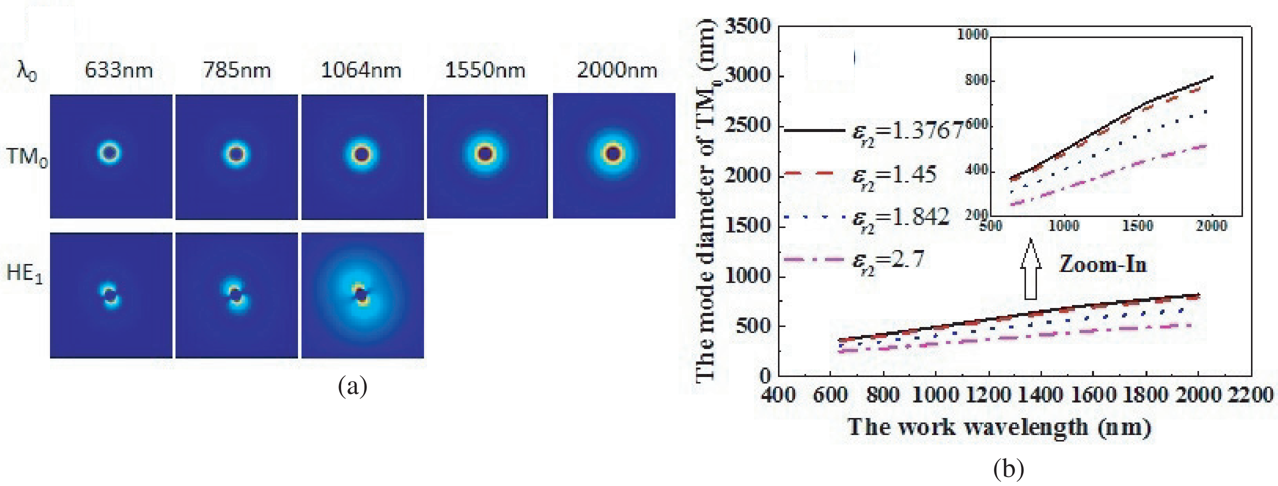

Figure 4. (a) $|E|$ mode patterns for all supported modes by metal nanowires with $a = 100$ nm and $\varepsilon_{r2} = 1.45^2$; (b) Curves of mode field diameters with the work wavelengths and permittivity of cladding dielectric.

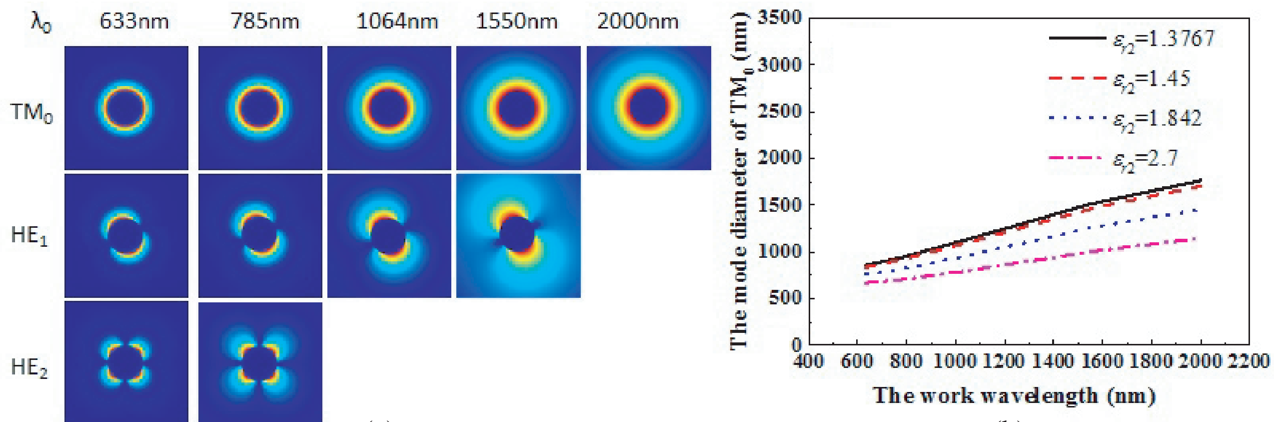

(a) (b)

Figure 5. (a) $|E|$ mode patterns for all supported modes by metal nanowires with $a = 300\,\text{nm}$ and $\varepsilon_{r2} = 1.45^2$; (b) Curves of mode field diameters with the work wavelengths and permittivity of cladding dielectric.

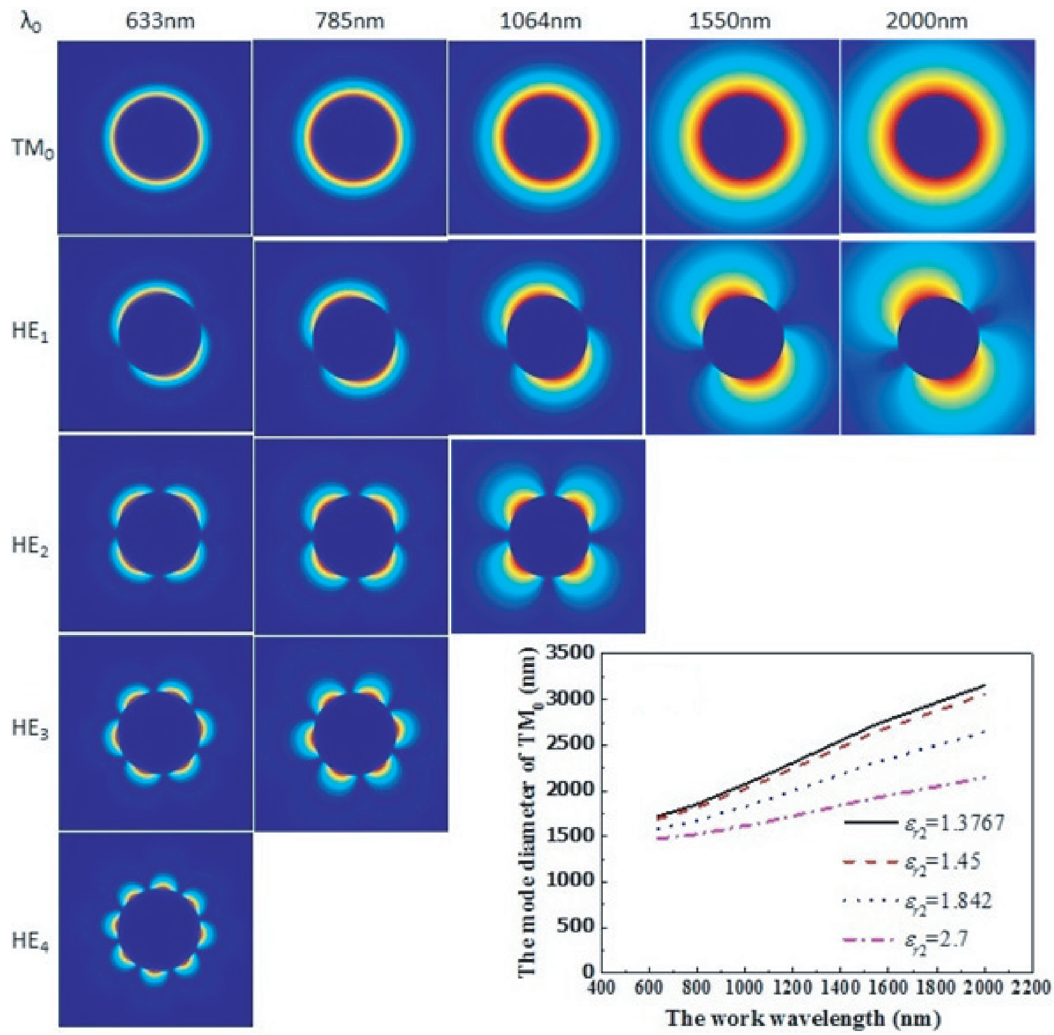

(a) (b)

Figure 6. (a) $|E|$ mode patterns for all supported modes by metal nanowires with $a = 700\,\text{nm}$ and $\varepsilon_{r2} = 1.45^2$; (b) Curves of mode field diameters with the work wavelengths and permittivity of cladding dielectric.

6. CONCLUSIONS

In conclusion, we have applied an analytical solution for evaluating SPPs modes supported by metal nanowires embedded in dielectric. We study single-mode propagation condition, mode field diameters of SPPs modes and the number of SPPS modes based on the dispersion equation. Our analytical method permits deeper insight into the mode behavior guided by metal nanowires for routing and controlling SPPs modes. Our results indicate that: (a) Only TM and HE SPPs modes can be guided in metal nanowires, and TM modes always exist; (b) HE modes have cutoff conditions, and the metal nanowires with smaller core radius guide fewer SPPs modes while the work wavelength is fixed; (c) The single-mode propagation is determined by three parameters including the core radius a, permittivity of the cladding dielectric ε_{r2} and work wavelength λ_0. The single-mode propagation can be achieved by tuning one of them when the other two are fixed; (d) Longer work wavelength leads to fewer supported SPPs modes and larger mode field diameters; (e) Mode field diameters increase with the increase of the core radius a and the decrease of the permittivity of the cladding dielectric ε_{r2}. All these results are valuable for achieving single-mode propagation and designing integrated plasmonic circuits based on metal nanowire.

ACKNOWLEDGMENT

This work was supported by the National Natural Science Foundation of China (No. 61405083); The Fundamental Research Funds for the Central Universities (lzujbky-2016-134, lzujbky-2016-135, lzujbky-2016-137).

REFERENCES

1. Gramotnev, D. K. and S. I. Bozhevolnyi, "Plasmonics beyond the diffraction limit," *Nature Photonics*, Vol. 4, No. 2, 83–91, 2010.
2. Barnes, W. L., A. Dereux, and T. W. Ebbesen, "Surface plasmon subwavelength optics," *Nature*, Vol. 424, No. 6950, 824, 2003.
3. Politano, A., et al., "Photothermal membrane distillation for seawater desalination," *Adv. Mater.*, Vol. 29, No. 2, 2017.
4. Politano, A., et al., "When plasmonics meets membrane technology," *Journal of Physics. Condensed Matter: An Institute of Physics Journal*, Vol. 28, No. 36, 363003, 2016.
5. Wang, Y. P., et al., "Single-mode plasmonic waveguiding properties of metal nanowires with dielectric substrates," *Optics Express*, Vol. 20, No. 17, 19006–1915, 2012.
6. Sanders, A. W., et al., "Observation of plasmon propagation, redirection, and fan-out in silver nanowires," *Nano Lett.*, Vol. 6, No. 8, 1822, 2006.
7. Li, Z. P., et al., "Effect of a proximal substrate on plasmon propagation in silver nanowires," *Physical Review B*, Vol. 82, No. 24, 2762–2768, 2010.
8. Ditlbacher, H., et al., "Silver nanowires as surface plasmon resonators," *Physical Review Letters*, Vol. 95, No. 25, 257403, 2005.
9. Shegai, T., et al., "Unidirectional broadband light emission from supported plasmonic nanowires," *Nano Lett.*, Vol. 11, No. 2, 706–711, 2011.
10. Li, Z., et al., "Directional light emission from propagating surface plasmons of silver nanowires," *Nano Lett.*, Vol. 9, No. 12, 4383, 2009.
11. Fang, Y. R., et al., "Branched silver nanowires as controllable plasmon routers," *Nano Lett.*, Vol. 10, No. 5, 1950, 2010.
12. Yan, R., et al., "Direct photonic-plasmonic coupling and routing in single nanowires," *Proc. Natl. Acad. Sci. USA*, Vol. 106, No. 50, 21045, 2009.
13. Wei, H., et al., "Cascaded logic gates in nanophotonic plasmon networks," *Nat. Commun.*, Vol. 2, No. 2, 387, 2011.

14. Viti, L., et al., "Efficient Terahertz detection in black-phosphorus nano-transistors with selective and controllable plasma-wave, bolometric and thermoelectric response," *Scientific Reports*, Vol. 6, 20474, 2016.
15. Viti, L., et al., "Plasma-wave Terahertz detection mediated by topological insulators surface states," *Nano Lett.*, Vol. 16, No. 1, 80, 2016.
16. Li, Q. and M. Qiu, "Plasmonic wave propagation in silver nanowires: guiding modes or not?," *Optics Express*, Vol. 21, No. 7, 8587, 2013.
17. Pan, D., et al., "Mode conversion of propagating surface plasmons in nanophotonic networks induced by structural symmetry breaking," *Scientific Reports*, Vol. 4, No. 4, 4993, 2014.
18. Zou, C. L., et al., "Plasmon modes of silver nanowire on a silica substrate," *Applied Physics Letters*, Vol. 97, No. 18, 189, 2010.
19. Paschotta, R. D., *Encyclopedia of Laser Physics and Technology*, Wiley-VCH, Weinheim, 2008.
20. Suffczyński, M., "Optical properties of the noble metals," *Physica Status Solidi (B)*, Vol. 4, No. 1, 3–29, 1964.